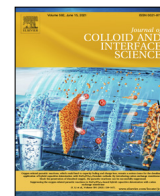




Contents lists available at ScienceDirect

Journal of Colloid and Interface Science

journal homepage: www.elsevier.com/locate/jcis

Regular Article

Oligonucleotide sensor based on magnetic capture and photoligation of upconverting nanoparticles in solid surfaces



Diego Mendez-Gonzalez ^{a,*}, Pedro P. Silva-Ibáñez ^{a,b}, Fernando Valiente-Dies ^{c,a}, Oscar G. Calderón ^d, Juan L. Mendez-Gonzalez ^e, Marco Laurenti ^{a,g,h}, Ana Egatz-Gómez ^{d,f}, Elena Díaz ^c, Jorge Rubio-Retama ^a, Sonia Melle ^{d,*}

^a Department of Chemistry in Pharmaceutical Sciences, Complutense University of Madrid, E-28040 Madrid, Spain

^b Department of Animal Science, University of Concepción, Chillán, Chile

^c GISC, Department of Materials Physics, Complutense University of Madrid, E-28040 Madrid, Spain

^d Department of Optics, Complutense University of Madrid, E-28037 Madrid, Spain

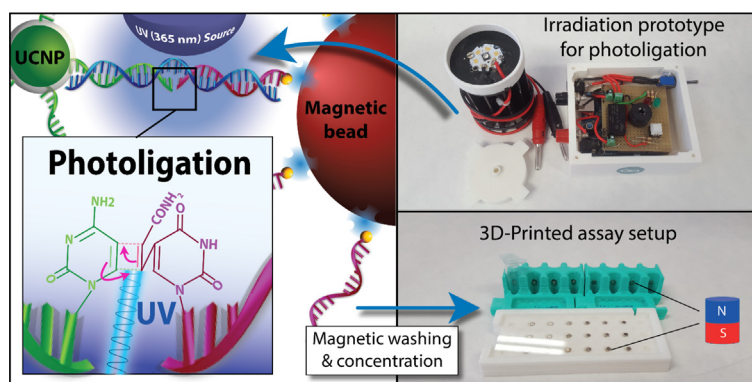
^e Institute of Optics, Consejo Superior de Investigaciones Científicas (CSIC), E-28006 Madrid, Spain

^f Center for Applied Structural Discovery, The Biodesign Institute, Arizona State University, Tempe, AZ 85281, United States

^g Instituto de Ciencia de Materiales de Madrid, c/Sor Juana Inés de la Cruz, Cantoblanco, 28049 Madrid, Spain

^h Instituto Ramón y Cajal de Investigación Sanitaria, Hospital Universitario Ramón y Cajal, 28034 Madrid, Spain

GRAPHICAL ABSTRACT



ARTICLE INFO

Article history:

Received 6 October 2020

Revised 25 January 2021

Accepted 21 February 2021

Available online 11 March 2021

Keywords:

Upconverting nanoparticles

Magnetic microparticles

DNA detection

ABSTRACT

In this work, we present a luminescence platform that can be used as point of care system for determining the presence and concentration of specific oligonucleotide sequences. This sensor exhibited a limit of detection as low as 50 fM by means of: (i) the use of single-stranded DNA (ssDNA) functionalized magnetic microparticles that captured and concentrated ssDNA-upconverting nanoparticles (ssDNA-UCNPs) on a solid support, when the target sequence (miR-21-5p DNA-analogue) was in the sample, and (ii) a photoligation reaction that covalently linked the ssDNA-UCNPs and the ssDNA magnetic microparticles, allowing stringent washes. The presented sensor showed a similar limit of detection when the assays were conducted in samples containing total miRNA extracted from human serum, demonstrating its suitability for detecting small specific oligonucleotide sequences under real-like conditions. The strategy of

* Corresponding authors.

E-mail addresses: diegomen@ucm.es (D. Mendez-Gonzalez), smelle@fis.ucm.es (S. Melle).

Photoligation
Magnetic capture
Magnetic concentration
Biosensor

combining UCNPs, magnetic microparticles, and a photoligation reaction provides new insight into low-cost, rapid, and ultra-sensitive detection of oligonucleotide sequences.

© 2021 Elsevier Inc. All rights reserved.

1. Introduction

Short non-coding oligonucleotide sequences such as miRNAs are considered as biomarkers for diagnosis and prognosis of many different diseases such as cancer [1], neurodegenerative diseases [2], or viral infections [3,4], just to mention a few. The importance of detecting short non-coding oligonucleotides lies in the fact that changes in the miRNA profiles can become apparent before the disease manifests itself, and for this reason they can be used in early diagnosis [5,6]. Furthermore, variations in the concentration profile of different short non-coding oligonucleotide sequences can be used to determine the evolution of the disease and can help to modify or adopt new treatments [7–9]. However, the detection and quantification of short non-coding oligonucleotide sequences is not trivial and most of these analyses have to be carried out by qRT-PCR or next-generation sequencing. These techniques can be considered as the gold standard, however, they require specialized laboratories equipped with expensive instrumentation that are handled by well-trained personnel. For these reasons, the development of alternative methods that could be used as screening tools in the detection of short non-coding oligonucleotide sequences could be a leap forward in the development of DNA/RNA sensors suitable as effective and rapid point of care (POC) diagnostics, which circumvent bottlenecks related with enzymatic transcription and amplification methods, as well as their time-consuming and equipment-associated costs [10–12].

Highly sensitive assays based on upconverting nanoparticles for detecting the presence of tiny concentrations of biological targets such as antigens, antibodies, oligonucleotides and pathogens have been reported [13–16]. This stunning detection ability is related to the capacity of UCNPs to absorb low-energy photons in the near infrared (NIR) range and emit higher-energy photons in the UV–vis region in exchange. This anti-Stokes emission is a unique optical phenomenon unobserved in biological samples, allowing measurements free of autofluorescence and with reduced scattered light [17,18]. In addition, the large anti-Stokes shifts, narrow emission bands, the possibility to tune their emission, elevated photostability, lack of photobleaching and photoblinking favor highly sensitive assays [19–21]. In these biosensors, UCNPs conjugated to ssDNA probes, which are complementary to a partial region of the target, act as specific reporters towards the presence of the target sequence upon hybridization. Subsequently, the target and the functionalized UCNPs can then be captured on a solid support modified with an additional ssDNA, upon its hybridization with the remaining region within the target sequence. Thus, the capture of target-ssDNA-UCNPs complexes by the probe-functionalized solid support is proportional to the target concentration present in the media [22–24].

An attractive solid support, for quick capture of target biomolecules, are magnetic particles due to their high specific surface area that favor a high local target concentration at their surface [25,26]. Additionally, their magnetic properties allow them to be recovered, repeatedly washed, and concentrated into small volumes to improve assay sensitivity [24,27]. In fact, the combination of ssDNA-functionalized magnetic particles for selective recognition and concentration of ssDNA-UCNPs used as luminescent reporters, has been tested for the sensitive detection of circulating tumor cells [28], potential biomarkers for Alzheimer's disease diagnosis as $A\beta$ oligomers [29], small molecules as mycotoxin ochratoxin A [30], insecticides as acetamiprid [31], glyco-biomarkers as carcinoembryonic antigen [32], non amplified DNA detection [33–36] as well as in

PCR amplified DNA detection [37]. In these assays, magnetic particles allow a highly efficient magnetic bio-separation and concentration of the target, which makes it possible to detect target concentrations around the pM range by measuring the luminescence of UCNPs. One of the first examples of a nucleic acid detection assay using DNA functionalized UCNPs as reporter probes is the work by Wollenberger et al. The system was developed for the detection of the target ssDNA molecules M13mp18(+) at pM concentration (limit of detection (LOD) c.a. 240–120 pM) [33].

A major factor limiting sensitivity of UCNPs assays that capture the analyte onto a solid support is the undesired luminescent signal generated by non-specifically adsorbed ssDNA-UCNPs on the support surface, which worsens the signal-to-background ratio (S/B ratio) and the LOD of the assays. In a recent work, we have demonstrated how the use of a photochemical ligation reaction can highly improve the LOD in UCNPs-based assays using streptavidin-coated microwells [15]. This is achieved by the photochemical formation of a covalent link between the two ssDNA sequences that hybridize with the target sequences. This link stabilizes the DNA bridge between the microwell and the UCNPs and allows to apply stringent washing to remove the non-specifically bound UCNPs, reducing the background signal and improving the LOD and the resulting sensitivity of the assay.

In this work we developed a cost-efficient and ultrasensitive DNA sensor, whose portable assay setup was designed to be quickly built using 3D-printing technologies. The working mechanism of the assay is based on the selective capture of ssDNA-UCNPs by ssDNA-magnetic microparticles, when a specific target sequence is present in the sample. For that, both particles were functionalized each one with a different type of ssDNA sequences that is partially complementary with the target sequence, a DNA-analogue of microRNA miR-21-5p. Thus, in the presence of target sequences, the ssDNA strands anchored on the UCNPs and the magnetic microparticles hybridize with these sequences, forming complexes that are simultaneously magnetic and luminescent. Beside that, the hybridization brings in close proximity and with a proper orientation the ssDNA anchored on both particles (see Fig. 1). This situation allows an efficient photochemical ligation between these ssDNA strands, upon irradiation with UV light. This reaction yields a covalent linkage of the UCNPs to the magnetic microparticles, which allows to apply harsh washings to the complexes that aim to remove the non-specifically bound ssDNA-UCNPs before to magnetically concentrate them on a solid surface, improving the S/B ratio and the LOD of the assay. Furthermore, we evaluated the effect that the size of the UCNPs produces in the analytical properties of the sensor. The validity of the system was checked in samples containing total microRNA extracts from the serum of healthy patients, which were spiked-in with different concentrations of miR-21-5p DNA-analogue. Finally, we have theoretically reproduced the experimental response of our sensor by means of the Hill-Lagmuir equation [38,39] and the effect of the non-specific binding, which provides an estimation of the LOD.

2. Materials and methods

2.1. Chemicals

Ytterbium (III) chloride hexahydrate (99.9%), yttrium (III) chloride hexahydrate (99.9%), erbium (III) chloride hexahydrate

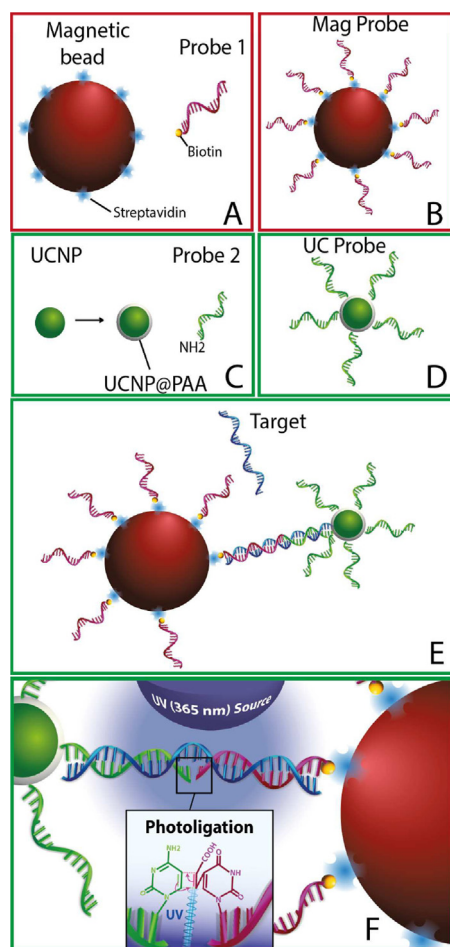


Fig. 1. (A–B) Mag Probes are 1 μm streptavidin magnetic beads bound to a photoactivatable and biotinylated ssDNA probe 1. (C–D) UC Probes are UCNP@PAA functionalized with the ssDNA probe 2. (E) miRNA target is captured with the UC Probe and the Mag Probe. (F) UV irradiation to photoligate the ssDNA strands from the Mag Probe and the UC Probe that were hybridized with the target.

(99.9%), 1-octadecene (90%), oleic acid (90%), sodium hydroxide (98%), ammonium fluoride (99.9%), methanol (99.9%), n-hexane (95%), N-(3-(dimethylamino) propyl)-N'-ethylcarbodiimide hydrochloride (99%), N-hydroxysulfosuccinimide sodium salt (98%), polyacrylic acid (PAA) (Mw~2000; 50 wt in H_2O), 2-(N-morpholino) ethanesulfonic acid (MES) (99%), Tris HCl (99%), bovine serum albumin (BSA) (96%), Tween 20 (BioXtra) (100%), Tween 40 (BioXtra) (90%), NaN_3 (99.5%), diethylenetriaminepentaacetic acid (DTPA) (98%), ethylenediaminetetraacetic acid (EDTA) (99%), and Sodium Chloride (NaCl) (99.5%) were purchased from Sigma–Aldrich and used as received. All chemicals were of analytical grade and were used as received without further purification.

Superparamagnetic $\gamma\text{-Fe}_2\text{O}_3$ polystyrene microparticles were purchased from Invitrogen (Dynabeads™ MyOne Streptavidin T₁,

Table 1
DNA sequences used in this work.

Name	Sequence
Biotin-modified photoactivatable probe for bioconjugation with streptavidin magnetic particles, probe 1	5' [cvU] GAT AAG CTA [Biotin]-3'
Amino-modified probe for bioconjugation with UCNP@PAA, probe 2	5' $\text{NH}_2\text{-C}(6)\text{-TCA ACA TCA GTC -3'}$
miR-21-5p DNA-analogue, Target	5'-TAG CTT ATC AGA CTG ATG TTG A-3'

cat.No. 65601). Typical binding capacity for 1 mg of Dynabeads is approximately 400 pmol of ss oligonucleotides (i.e. around 25×10^4 ss oligonucleotides/magnetic bead). ssDNA probe 1 was a biotin modified ssDNA sequence containing a photoactivatable nucleotide (5-carboxyvinyl-2'-deoxyuridine, or cvU) that was acquired from Bio-Synthesis Inc while probe 2 was an amino-modified ssDNA from Biomers.net GmbH. The complementary target used was a DNA-analogue of miR-21-5p from Biomers.net GmbH (see sequences in Table 1). Extraction of total miRNA from human serum was performed by using 'miRNeasy Mini Kit' from Qiagen©, and by following the protocol provided within.

2.2. 3D printing of magnetic rack and magnetic array cartridge

The rack for magnetic separation of the magnetic beads and the cartridge containing a magnetic array for magnetic concentration of magnetic beads in a solid support were printed by using a Legio 3D printer (Leon3D). The printing dimensions (XYZ) are 200 x 200 x 200 mm, the maximum resolution (printing nozzle 0.4 mm) was given by a minimum layer width of 0.05 mm, and the printing speed can be chosen between 90–250 mm/s. This model was equipped with thermistors EPCOS 100 K, and a heated bed. The extruder was a "HotEnd" type All-metal LeoNozzle V2, with a ceramic cartridge of 12 V/40 W. The filament diameter was 1.75 mm and the heating time was approximately 2 min. For further details regarding the printing parameters, the 3D software used to modify and to do the slicing of the models, and for downloading the STL files ready available for printing the setup used in this work, see Supplementary Information S1 and S2.

2.3. Mag Probe: functionalization of magnetic microparticle with ssDNA photoactivatable probe

The preliminary washes of Dynabeads™ magnetic microparticles, as well as during their process of functionalization with Probe 1 to form the Mag Probes, and later on during the detection assays, were performed by using a 3D-printed home-made magnetic rack (see Section S1 of Supplementary Information). This allowed the magnetic recovery of the magnetic microparticles, by magnetically concentrating them at the lateral wall of the eppendorfs (see Fig. S1). The magnetic microparticles preliminary washes were done as follows: First, 10 μL of Dynabeads™ T₁ (10 mg/mL) were added to 90 μL of Milli-Q H_2O to have a final volume of 100 μL . After this, 5 washes were performed with 100 μL of the Binding & Washing buffer 2x [B&W buffer 2x: 10 mM Tris-HCl, 1 mM of EDTA, 2 M of NaCl and 0.1% of Tween 20 (pH adjusted to 7.5)] provided with the beads by using the magnetic rack. The pellet was finally resuspended in 50 μL of B&W buffer 2x (hereinafter DB50). Then, the photoactivatable Probe 1 was immobilized on the Dynabeads™ surface as follows: 4 μL of a 10 μM Probe 1 stock solution were taken and added to 96 μL of sterile dd H_2O . Secondly, 50 μL of B&W buffer 2x were added to DB50. Then, both solutions were mixed to have a final volume of 200 μL . The mixture was incubated for 15 min at RT. After that, Mag Probes (that has just been formed) were recovered with the magnetic rack during 5 min. The supernatant was carefully removed, and the pellet was resuspended in 100 μL of B&W buffer 1x. The process was repeated 3 times. At the end, the pellet was resuspended in 50 μL of assay buffer [50 mM of Tris HCl, 0.5% of BSA, 0.01% of Tween 40, 0.5% of NaN_3 and 20 μM of DTPA (pH adjusted to 7.75), 0.5 M NaCl] (see Mag Probe in Figs. 1A and 1B).

2.4. Synthesis of $\text{NaY}_{0.78}\text{F}_4\text{:Yb}_{0.2}\text{Er}_{0.02}$ nanoparticles

$\text{NaY}_{0.78}\text{F}_4\text{:Yb}_{0.2}\text{Er}_{0.02}$ UCNP's were synthesized using the thermal coprecipitation method. [40] 236 mg of $\text{YCl}_3 \cdot 6\text{H}_2\text{O}$, 78 mg of

$\text{YbCl}_3 \cdot 6\text{H}_2\text{O}$, 7.8 mg of $\text{ErCl}_3 \cdot 6\text{H}_2\text{O}$, 15 mL of 1-octadecene, and 6 mL of oleic acid were placed in a 100 mL three necked round-bottom flask. The solution was heated to 140°C under moderate stirring and nitrogen atmosphere until all solids were dissolved. Then, the solution was cooled to room temperature (RT) and 10 mL of CH_3OH solution containing 110 mg of NaOH and 157 mg of NH_4F were added dropwise under vigorous magnetic stirring. The mixture was stirred for 15 min, then heated to 80°C for 20 min under a nitrogen flow, and finally at 80°C for 10 min under vacuum to remove $\text{H}_2\text{O}/\text{CH}_3\text{OH}$ traces. The flask was then heated to 320°C at a heating rate of $20^\circ\text{C}/\text{min}$ under a nitrogen atmosphere. The final temperature of 320°C was maintained for 45 min. Finally, the solution was cooled to RT and split into 4 tubes. Then, 4 mL of CH_3OH were added to each one, shaken, and let the two resulting phases to separate. After this, the methanol phase was removed, and the process was repeated twice more. Then, the remaining oily phase was centrifuged at 7269 g for 10 min, the supernatant was removed, and the resulting pellets were rinsed with 2 mL of ethanol, without dispersing them. This last process was repeated one more time. Finally, the pellets were let to dry for 2 min at RT, dispersed in 2.5 mL of n-hexane, and stored together in a glass vial for further use. The procedure to obtain bigger nanoparticles of $\text{NaY}_{0.78}\text{F}_4$: $\text{Yb}_{0.2}\text{Er}_{0.02}$ was exactly the same, except for that the CH_3OH solution containing the 110 mg NaOH and 157 mg NH_4F was aged for a week before its use.

2.5. Preparation of UCNP@PAA

A small n-hexane aliquot, containing 5 mg of UCNPs, was taken and centrifuged at 14000 g for 20 min. The supernatant was discarded and the resulting pellet was dried in order to remove the remaining solvent traces. The pellet was resuspended in 1 mL of HCl 0.1 M by ultrasonication (10 min) and stirred for 5 h using an orbital shaker. Then, the sample was centrifuged again at 21000 g for 20 min. The resulting pellet was resuspended in 1 mL of Milli-Q H_2O and centrifuged at 21000 g for 20 min. The supernatant was removed and 1 mL of polyacrylic acid (PAA) 2.5% wt solution (pH = 9) was added. The pellet was resuspended by sonication and stirred overnight at RT with an orbital shaker. After that, the solution was centrifuged at 21000 g for 20 min and the pellet was redispersed in 1 mL of deionized water; this process was repeated once. Then, the resulting pellet was redispersed in 0.5 mL of 2-(N-morpholino) ethanesulfonic acid (i.e. MES) buffer (pH = 6.1), centrifuged at 21000 g for 20 min, and finally resuspended in 0.25 mL of MES buffer 20 mM and stored at 4°C .

2.6. UC Probe: oligonucleotide conjugation protocol to UCNP@PAA

2.5 mg of UCNP@PAA were redispersed by sonication in 230 μL of MES 20 mM (pH = 6.5). After that, 10 μL of ssDNA (Probe 2) (5 nmol) were added to the solution. Then, 5 μL of EDC-HCl (1 M in MES buffer; 1.99 mg in 10 μL) and 5 μL of N-hydroxysulfosuccinimide (sulfo-NHS) (3 M in MES buffer; 3.39 mg in 10 μL) were added and vortexed for 3 min. The final mix was incubated for 2.5 h under slow stirring at RT. The EDC/sulfo-NHS coupling reaction was quenched by the addition of 6.25 μL of Glycine (2 M, pH = 11), vortexed and then incubated for 30 min. The resulting UCNP@PAA@ssDNA were centrifuged at 21000 g for 10 min, redispersed in 500 μL of buffer [10 mM of Tris HCl and 0.1% of Tween 20 (pH = 8.5)] and centrifuged again at 21000 g for 10 min. This step is repeated one more time. Finally, the conjugated UCNPs were redispersed in 244 μL of buffer [5 mM of Tris HCl, 0.2% of Tween 20, 50 μM of EDTA and 0.05% of NaN_3] and 6.25 μL of BSA (20% wt) were added (see UC Probe in Fig. 1C and 1D).

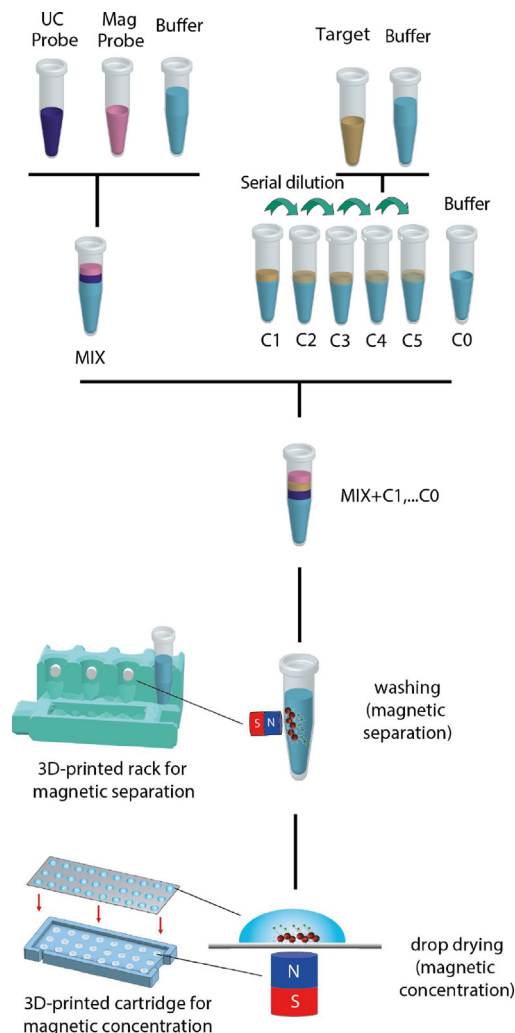


Fig. 2. Procedure to develop an assay for oligonucleotide detection on a solid support.

2.7. Assay protocol for the detection of miR-21-5p

Serial dilution of miR-21-5p DNA target (see procedure in Fig. 2): 6 different eppendorf tubes were filled-up with 50 μL of assay buffer. Then, 5.5 μL of the target (miR-21-5p) at 10 nM were added to the first eppendorf tube C1, and the solution was vigorously shaken. In the next steps, 5.5 μL were taken from the last dilution of target prepared up to that point (e.g. C1 in this case) and added to the next eppendorf (e.g. C2) and shaken, in order to continue the 10x serial dilution. This process was repeated until all serial dilutions were completed. In the last dilution (i.e. C5) 5.5 μL of the resulting solution were discarded to maintain the same volume as in previous eppendorfs. The 6th eppendorf (C6) contains only 50 μL of buffer (i.e. without target sequence), to be used as negative control. The resulting eppendorf tubes were named as follows: C1 (500 pM), C2 (50 pM), C3 (5 pM), C4 (0.5 pM), C5 (0.05 pM), and C6 (no target).

After that, a mix was prepared by mixing 35 μL of UC Probe at 100 $\mu\text{g}/\text{mL}$, 30 μL of Mag Probe at 2 mg/mL and 385 μL of assay buffer (hereafter referred as MIX). Then, 50 μL of the MIX were added to each of the previously prepared 6 eppendorf tubes. At this point, each eppendorf contains 3.8 $\mu\text{g}/\text{mL}$ of UC Probe and 65 $\mu\text{g}/\text{mL}$ of Mag Probe in a final volume of 100 μL . That means a molar concentration of 4.8 pM for UC Probes (estimated using the molecular weight of the hexagonal UCNPs [41]) and 0.1 pM for Mag

Probes (from its nominal value), i.e., a ratio of 48 UC Probes per Mag Probe which roughly covers the surface of the Mag Probe. The six eppendorf tubes were incubated for 2 h. After the incubation, 3 cycles of wash with 100 μL of assay buffer were performed using the magnetic separation rack (5 min). This served to recover by magnetic separation the UC Probes that had been specifically captured to the surface of the Mag Probe by means of hybridization with the target sequence (see complexes in Fig. 1E), while removing the ones that had not hybridized and were still in solution.

Once the complexes were concentrated in the form of a pellet at the eppendorf wall, the supernatant was removed and the pellet resuspended in 100 μL of assay buffer. This process was repeated 3 times. Each eppendorf was placed for 10 min in the magnetic rack to concentrate the magnetic particles at the eppendorf wall. After the last wash, the pellet was resuspended in 25 μL of assay buffer and homogenized.

2.8. DNA detection procedure on a solid support

At least three different 5 μL drops (replicas) from each of the 6 eppendorfs were deposited onto a microscope glass coverslip, which was previously placed on a home-made 3D-printed cartridge containing an array of small neodymium magnets of 2 mm in diameter (see details in Section S2 of Supplementary Information). The position of each of the drops placed at the coverslip corresponded to the position of a small magnet behind, which served to concentrate the Mag Probe-complexes formed during the assay, upon hybridization of the probes with the target, into a small spot. These magnets enable the pellet to concentrate in a 2 mm-diameter area around the center of the drop (drop diameter \simeq 4 mm), allowing the amplification of the luminescent signal (i.e. more luminescence per area) and simplifying the acquisition of representative measurements from the samples (i.e. the luminescence produced by the whole spot is read with just a few measurements).

2.9. DNA photochemical ligation to Mag Probe procedure

To improve the LOD of the assay, we proceeded to photoligate the ssDNA strands from the Mag Probe and the UC Probe, which were held facing each other upon hybridization with the target. The target sequence brings in close proximity the UC Probe and the photoactivatable Mag Probe upon hybridization. Under this scenario, the cytosine at the 3' end in UC Probe faces the photoactivatable nucleotide 5-carboxyvinyl-2'-deoxyuridine (cvU), located at the 5' end in Mag Probe. At this point, the spatial conformation and close proximity allows the selective photochemical ligation reaction between both nucleotides upon UV irradiation (see Fig. 1F). In this regard, previous works have demonstrated that no photoligation occurs in the absence of target template, highlighting to which extent these photochemical reactions are clean and highly selective to the presence of the target [42–44]. A 2.7 W LED (Engin LZ1-00UV00 365 nm) with emission centered at 365 nm was used as UV light source to trigger the photochemical ligation reaction. After the incubation time, we used a custom-made adapter to fix the UV LED on top of the uncapped eppendorf tubes for direct irradiation, during 5 min, of the samples contained within (more details in Section S3 of Supplementary Information). During the photoligation process the tubes were refrigerated at 10°C. This photoligation step allowed the use of more stringent washes in order to remove the UC Probes non-specifically bound to Mag Probes, due to the target-specific formation of a strong covalent union between both probes. For this reason, in this case it was possible to perform three washing steps with 400 μL of assay buffer, without negatively affecting the signal to background ratio. The cleaned pellets were dispersed in a final

volume of 25 μL of assay buffer, homogenized, and several replicas deposited on the glass support for magnetic concentration and later luminescence measurement.

2.10. Detection assay in total miRNA extracted from human serum

Total miRNA was extracted from 500 μL of human serum from healthy patients using miRNAeasy Mini Kit protocol from Qiagen©. A total amount of 2.7 μg of miRNA was extracted using this process. After the extraction, the extracted miRNA was diluted to 285 μL of assay buffer (9.5 ng/ μL of miRNA) to act as a pool of background miRNA. The resulting dilution was splitted into 5 different eppendorfs. An additional eppendorf was prepared containing only assay buffer (eppendorf 6th). Then, 4 out of the 5 eppendorf containing the extracted total miRNA were doped with different concentration of the miR-21-5p DNA-analogue target sequence, as in previous experiments. Then, 50 μL of the MIX (at the same concentration as used in the previous experiments) were added to each one of the 6 eppendorf tubes. Here, the eppendorf 6th, containing only assay buffer (without total miRNA extracted from human serum) and UC Probe + Mag Probe mixture, served as an additional negative control (no target spiked-in). It allowed us to estimate the possible contribution that the endogenous miR-21-5p naturally present in human serum may have in the luminescent signal of negative control doped with total miRNA extracted from human serum (eppendorf 5th) due to hybridization of UC Probe and Mag Probe.

2.11. Morphological characterization

Electron microscopy images were acquired in transmission mode (TEM) using a JEM 1010 microscope (JEOL, Japan) working at 80 kV and equipped with a Gatan (USA) digital camera (model 782).

2.12. Z-potential measurements

All Z-potential experiments were performed using a Malvern Nano-ZS instrument (Malvern Instruments, United Kingdom). Before the Z-potential measurements, the samples were freshly prepared by diluting them to a final concentration of ca. 50 $\mu\text{g}/\text{mL}$. All measurements were obtained at 25°C by using the automatic mode (10 minimum runs 100 maximum runs), an equilibration time of 120 s, and the Smoluchowski fit model. A minimum of 3 independent measurements were performed for each sample.

2.13. Optical characterization

The emission of the UCNPs was measured with an upconversion fluorescence home-built system (see details in Fig. S4 of Supplementary Information). The excitation laser beam comes from a pig-tailed 10 W CW laser (JDSU, L4-9897603) operating at 976 nm and provided with a current and temperature controller (ILX Lightwave, LDX-36025-12 and LDT-5525B, respectively). The laser beam was transmitted through a long-pass dichroic filter (Semrock, FF757-Di01), and then focused on the sample with a 10X objective. The upconversion luminescence coming from the sample was reflected by the dichroic mirror towards two short-pass filters, which block the IR reflected radiation (Semrock, FF01-775/SP, and Thorlabs FESH0750). Then, the beam was focused into an optical fiber connected to a monochromator (Horiba Jobin Yvon, iHR320). The monochromator was equipped with a photomultiplier tube (Hamamatsu, R928) and used a 1800 gr/mm grating blazed at 500 nm. In order to characterize the laser power density at the sample, we measured the laser power with a thermal sensor power meter (Thorlabs, S310C) and the beam size (FWHM) using the slit scan

technique [45] being the beam size around 300 μm . In our measurements, we used an excitation laser power density on the sample between 0.4 and 1.3 kW/cm^2 . This allowed us to ensure that the laser operated below the excitation saturation power density of the transition ${}^2F_{7/2} \rightarrow {}^2F_{5/2}$ of the Yb^{3+} ions (see Fig. S5 of Supplementary Information), which is $I_{\text{sat}} = \hbar\omega / (2\sigma^Y \tau^Y) = 3 \text{ kW}/\text{cm}^2$, where $\tau^Y = 2 \text{ ms}$ is the excited level lifetime, $\sigma^Y = 1.7 \times 10^{-20} \text{ cm}^2$ is the absorption cross-section, and $\hbar\omega$ the transition energy (resonant with the excitation laser wavelength at 976 nm).

Upconversion luminescence spectra of the target captured by the Mag Probe and the UC Probe were measured as follows: consecutive spectra were collected at different spots within the center of the same dried drop. An optical alignment system (composed by a lens, NIR neutral density filters and a CCD camera) was used to adjust the measuring spot at different positions within the pellet (see details in Fig. S4 of Supplementary Information). Three different drops were analyzed for each target concentration. Then, we computed the average intensity of the integrated area of the spectra within the red emission band which corresponds to the transition ${}^4F_{9/2} \rightarrow {}^4I_{15/2}$ of the Er^{3+} ions (see Fig. S5 of Supplementary Information), and we took the maximum deviation as the error.

3. Results and discussion

We synthesized oleate-capped $\text{NaY}_{0.78}\text{F}_4:\text{Yb}_{0.2},\text{Er}_{0.02}$ nanoparticles of two different sizes using the thermal co-precipitation method. TEM images show highly monodisperse spherical UCNPs with an average diameter of $35 \pm 2 \text{ nm}$ and hexagonal prism shaped UCNPs with an equivalent spherical diameter of $81 \pm 5 \text{ nm}$ (see dimensions in Fig. 3). Then, we coated the UCNPs with PAA through ligand exchange. After PAA modification, the nanoparticles became water-dispersible, showing good colloidal stability due to their surface negative charges (ζ -potential of -21 mV). This is indicative of PAA's carboxylic acid deprotonation, confirming the presence of the $-\text{COOH}$ groups from PAA at the surface of the UCNPs (Fig. 1C). Then, probe 2 (ssDNA- NH_2) was grafted to the surface of UCNP-s@PAA by means of the EDC/Sulfo-NHS coupling reaction between the amino group of probe 2 and the carboxylic groups of UCNP-s@PAA, resulting in UC Probe, UCNP@sDNA (Fig. 1D).

To prepare the Mag Probes, a photoactivatable and biotinylated DNA probe, probe 1, was immobilized onto the surface of streptavidin-coated superparamagnetic beads (DynabeadsTM, 1 micron in diameter), by taking advantage of the high affinity between biotin and streptavidin (Fig. 1B). Once both probes have been prepared, UC Probes at $3.8 \mu\text{g}/\text{mL}$ and Mag Probes at $65 \mu\text{g}/\text{mL}$ (with a theoretical concentration of Probe 1 attached to the DynabeadsTM by biotin-streptavidin interaction of 25 nM) were

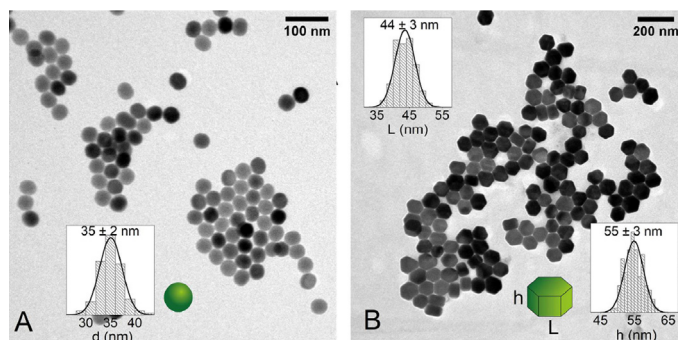


Fig. 3. TEM images of highly monodisperse β -phase synthesized $\text{NaYF}_4:\text{Yb},\text{Er}$ nanoparticles. (A) Spherical UCNPs with average diameter of $35 \pm 2 \text{ nm}$. (B) Hexagonal UCNPs with average side length of $44 \pm 3 \text{ nm}$ and height of $55 \pm 3 \text{ nm}$. Insets show the particle size histograms.

incubated at different concentrations of the miR-21-5p target (from 0.05 pM to 500 pM, and 0 target concentration as negative control) in assay buffer (final volume 100 μL) for 2 h to ensure that the hybridization equilibrium was achieved (see procedure in Fig. 2). We tested that larger incubation times lead to similar results. After that, three washes with 100 μL of assay buffer during 5 min were performed with the help of a 3D-printed home-made magnetic rack in order to remove the non-specifically bound UC Probes from the Mag Probes. Then, 5 μL drops were deposited on a glass coverslip placing the home-made 3D-printed cartridge underneath, which contained an array of magnets. This ensures the concentration of the hybridized complexes into a small spot at the bottom of each deposited drop for their subsequent measurement. The re-design of the 3D-models printed and presented in here (i.e. magnetic rack and cartridge) allowed us to miniaturize the setup, extend it on demand, or adjust it almost immediately and at an affordable price. This permitted us to test and quickly reach optimal specifications of the models to successfully improve the performance of the sensor, as we did in the case of the 3D-printed cartridge containing the magnetic array.

To analyze the performance of the sensor, we measured the luminescence spectra of the UC Probes that were captured and concentrated by Mag Probes upon hybridization with different target concentrations. As an example, Fig. 4A shows the red upconver-

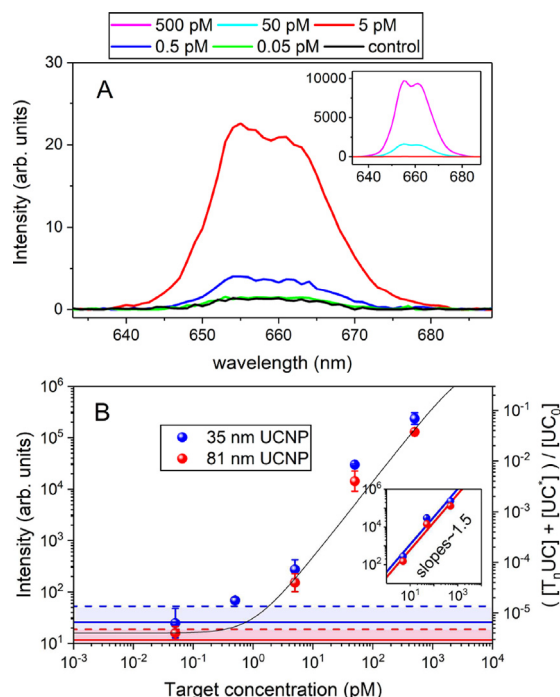


Fig. 4. (A) Red upconversion luminescence spectra for samples with 35 nm UC Probes generated by different target concentrations when excited with a $1.3 \text{ kW}/\text{cm}^2$ 976 nm laser. Black curve corresponds to zero target concentration so accounts for the luminescence signal coming from non-specifically bound UC Probes (background signal). The inset shows the highest considered target concentration. (B) Sensor calibration curve: Integrated intensity of the red emission band (left axis) versus target concentration for the UC Probes with 35 nm in diameter (blue circles) and 81 nm (red circles) at an excitation power density of $1.3 \text{ kW}/\text{cm}^2$ and $0.4 \text{ kW}/\text{cm}^2$, respectively. Error bars are the maximum deviation obtained from measurements at different positions on each pellet out of two or more independent pellets for each target concentration. Blue (red) solid horizontal line indicates the control luminescence of the zero target sample, while blue (red) dashed horizontal line indicates the LOD (defined as background signal + $3 \times \text{SD}$). (Inset) Linear fit ranging between 5 pM and 500 pM. (Right axis) Black line corresponds to the theoretical captured fraction of UCNPs versus the total target obtained from Eqs. 2 and 4. (For interpretation of the references to colour in this figure legend, the reader is referred to the web version of this article.)

sion luminescence spectra upon 976 nm excitation (1.3 kW/cm^2) from the captured 35 nm UC Probes. It is evident how the intensity of the spectra gradually increases above 0.5 pM, encompassing the increase of target concentration present within each sample. The presence of a higher amount of target sequences yields a higher number of UC NPs captured by the Mag Probes during the assay, which corresponded with a more intense luminescence signal after reading the magnetically concentrated pellets on the glass substrates. However, for a target concentration around 0.05 pM, the spectrum remains unresolved when compared with the one of the negative control sample (see green and black lines in Fig. 4A). Still, the sensor detects down to 0.5 pM of target sequence, demonstrating a relatively high sensitivity. In this regard, we found out that the magnetic concentration of the complexes after the deposition of the drops on the glass coverslip is an essential point allowing to detect luminescence signals for low target concentrations. In fact, in order to detect these very low levels of target, it is necessary to meet a proper compromise between the number of Mag Probes present in the drops, and the diameter of the magnets used in the array to form the pellets. Quite interestingly we found that both, the target detection without the magnetic concentration step of Mag Probes, or concentrating them into a very small area, were detrimental to detect the luminescence of small quantities of UC NPs. This can be explained by the reduced luminescent signal/per unit area when magnetic concentration is absent, and by a large variation of the spatial distribution of Mag Probes when magnets are too small, which hampers the detection of UC Probe luminescence. After trying different approaches and building arrays with several magnet diameters, we found out that 25 nm Mag Probe and a cartridge containing an array of 2 mm magnets allowed us to obtain a uniform Mag Probe spatial distribution (see Fig. S4 of Supplementary Information) and the aforementioned sensitivity (around 0.5 pM). In order to test the stability of the samples, we measured again some of the samples after a long period (close to a month), without finding any sign of degradation.

Fig. 4B shows the sensor calibration curve, where the integrated intensity of the UC Probes' red emission is depicted versus the target concentration. In this graph, the calibration curve for 35 nm UC NPs used as UC Probes (blue symbols) is compared with that obtained with the 81 nm UC NPs (red symbols), under 1.3 and 0.4 kW/cm^2 excitation power densities, respectively. Interestingly, a similar dependence with target concentration is found for both UC NPs sizes, whereas larger excitation power densities are required for the smaller UC Probes to be detected with similar luminescence signals. Very large nanoparticles (e.g. above 100 nm) have been reported to be detrimental as assay reporters, due to steric restrictions that can hamper the interaction between the UCNP reporter and the target, specially when hybridized with the solid phase (i.e. magnetic beads in our case), or by reducing the dynamic range of the sensor at high target concentrations, due to limited UCNP packing and steric restrictions/repulsive forces [46,47]. Nevertheless, in comparison with small nanoparticles, the use of moderately large sizes (i.e. smaller than 100 nm or 60 nm in diameter in some cases) seems to be accompanied with an improvement of assay performance, as the previous effects are not predominant yet. This is due to a combination of different factors such as i) allowing a higher number and stronger specific interactions with the target captured by the solid phase (i.e. magnetic beads), as bigger sizes will have larger surface areas and will contain more DNA probes at their surface, ii) a reduction of the assay background signal, as larger sizes will imply a reduction of the number of reporters if assuming a constant mass of NPs, and iii) a better detectability, as larger nanoparticles will provide a higher luminescence per target hybridization event [46,47]. The latter effect is especially relevant in our case, taking into account the steep increase of the UC NPs' quantum yield as a function of

their size (from 0.005% to 0.3% for 10 nm and 100 nm sizes, respectively) [48]. In fact, we found that using 81 nm UC NPs for this system is highly desirable, as it allows us to reduce more than 3 times the excitation power density required to reveal the luminescence of the assays, while maintaining similar assay performances. This allows the use of a less powerful, cheaper, and more portable excitation source, while lowers the risk of possible sample damage due to long term exposure at higher power densities. For this reason, we chose the 81 nm UC Probes as the luminescent reporters in all following experiments. We also plotted in Fig. 4B (dashed line) the minimum intensity value above which a target concentration is reliably detected, i.e. LOD, which is defined as the luminescence from the negative control (solid line) plus 3-fold its standard deviation (SD). Therefore, the lowest target concentration detected corresponds to 0.5 pM. The inset in Fig. 4B shows that a linear trend of the log–log plot calibration curve with slope 1.5 is obtained in the range of detection above 5 pM, extended within a range of more than two orders of magnitude. The slope value of 1.5 means that a relative change in target concentration of 10% leads to a relative variation in luminescence intensity around 15%. This slope gives a relative sensitivity of 30%/pM for a target concentration of 5 pM which is higher than the relative sensitivity values obtained in similar streptavidin coated solid support detection systems [24]. This relatively high sensitivity is very desirable for the early diagnosis of diseases by means of miRNA quantification. In fact, it implies that a relatively small change in miRNA concentration, such as those that occur in the expression levels of specific miRNAs in cancer patients compared with healthy ones, will have a relatively strong impact on the resulting luminescence signal, favoring the detection of this variation. The extrapolation of the linear trend to the LOD (dashed line in Fig. 4B) gives us an estimation for the lowest limit of target concentration that follows this linear trend, which is 0.9 pM for the 35 nm UC Probes and 1.2 pM for the 81 nm UC Probes.

The LOD achieved in the experiments (0.5 pM) is still around 5-times over the miR-21-5p concentrations reported by some authors for breast cancer patients (89–102 fM) [49]. Then, to further improve the LOD of the sensor, we proceeded to photoligate the ssDNA strands of the Mag Probes and the UC Probes that are held face to face upon hybridization with the target. This procedure stabilizes covalently the complex between the UC Probes and the Mag Probes and permits performing a more stringent cleaning procedure to reduce the number of those UC Probes that have non-specifically bound to Mag Probes. Thus, after the photoligation was triggered by irradiating the samples with UV light (640 mW/cm^2 , 5 min), the samples were washed with larger buffer volumes (400 μL instead of 100 μL), for longer times (10 min instead of 5 min) and collected using magnetic separation. To analyze the impact of the photoligation process in the target detection, we measured the luminescence spectra for samples with a target concentration of 0.05 pM and 0.5 pM together with the negative control sample. As shown in Fig. 5, larger luminescence signals than the ones obtained from the negative control (zero target concentration, black line in Fig. 5A) can be obtained for target concentrations as low as 0.05 pM thanks to the photoligation process. Fig. 5B shows the integrated fluorescence intensity of the samples used in Fig. 5A at two different excitation power densities 0.4 and 1.3 kW/cm^2 . The LOD achieved for both excitation power densities is shown in dashed lines in Fig. 5B, being in both cases below the signals corresponding to the lowest target concentration used (0.05 pM). This implies a LOD improvement of more than 10-fold by simply adding a quick (5 min) photoligation step.

3.1. Target detection in total miRNA extracted from human serum

Given the improvement in the LOD of the sensor due to the photoligation step, we further tested the potential applicability of the

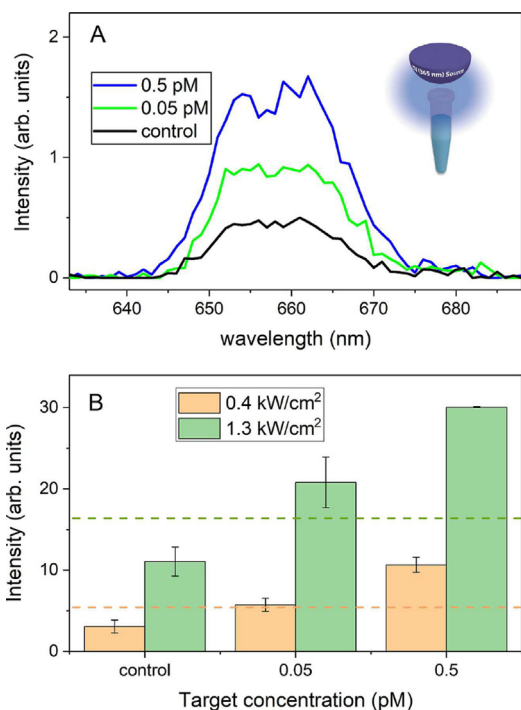


Fig. 5. LOD improves after photoligation. (A) Red upconversion luminescence spectra for samples with 81 nm UCNP and target sequences at very low concentrations excited with 1.3 kW/cm² 976 nm laser. Black curve corresponds to zero target concentration so accounts for non-specific binding. (B) Integrated intensity of the red emission band versus target concentration for different excitation power densities: 0.4 kW/cm² (brown) and 1.3 kW/cm² (green). After photoligation, four washes with 400 μ L of KGB 1x every 10 min were done to reduce non-specific binding. Error bars correspond to SD. Brown and green dashed lines show the LOD for 0.4 kW/cm² and 1.3 kW/cm² excitation power densities, respectively. (For interpretation of the references to colour in this figure legend, the reader is referred to the web version of this article.)

presented strategy in more realistic conditions. To do this, we studied the response of the sensor by detecting different concentrations of target in the presence of total miRNA extracted from human serum (used as a pool of background miRNA), which were added to the buffer solutions containing the different target concentrations aimed to be detected. Thus, an amount of 2.7 μ g of the extracted total miRNA was added (see Methods section for further details). Finally, the MIX containing UC Probe and Mag Probe was added to the eppendorf, as in previous experiments. We measured the luminescence for the different target concentrations following the same procedure and experimental conditions that yielded the results presented in Fig. 5 (2 h incubation, photoligation, and stringent washes with 400 μ L assay buffer). Results in Fig. 6 show that the main features found in the previous experiments remain. The calibration curve showed a linear trend in the log–log plot with a slope of 1.6 and a limit of detection below 0.05 pM. These results are practically identical to the one obtained in the same experiments carried out in buffers and demonstrate the negligible influence of the presence of the miRNA pool on the sensor response. Thus, the proposed sensor demonstrates potential for the direct detection of minute amounts of specific oligonucleotide sequences even in the presence of real miRNA pools extracted from the serum of healthy human patients. In this experiment, we exceptionally included two different controls: one negative control (blue dashed line) containing total miRNA extracted from serum, but lacking synthetic target sequence, which accounts for both the effect on the background signal coming from the possible hybridization with specific sequences from the miRNA pool (e.g. the endogenous miR-21-5p sequence naturally present in healthy patients) and also

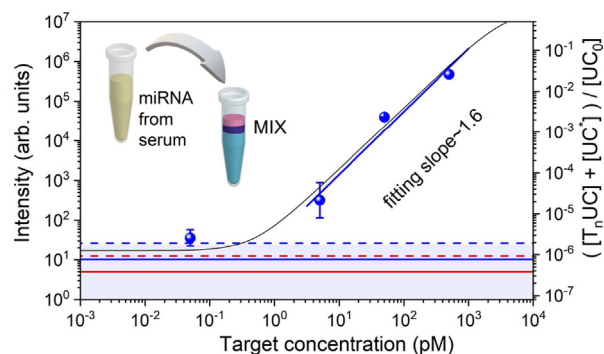


Fig. 6. Detection curve in total miRNA extracts from healthy human serum by using the photoligation step. (Left axis) Integrated intensity of the red emission band versus target concentration for the UC Probes with diameter 81 nm at excitation power density 0.9 kW/cm². Error bars are the maximum deviation obtained from measurements at different positions on each spot out of two independent samples for each target concentration. Linear fit is also shown. Solid horizontal lines indicate the luminescence of the zero target sample, while dashed horizontal lines indicate the LOD for the cases with (blue) and without (red) the miRNA extracts from human serum. (Right axis) Black line corresponds to the theoretical captured fraction of UCNP versus the total target obtained from Eqs. 2 and 4. (For interpretation of the references to colour in this figure legend, the reader is referred to the web version of this article.)

from the non-specific binding of UC Probes to Mag Probes; and another negative control, lacking both the miRNA pool and the synthetic target, which accounts only for the signal coming from the non-specific binding during the assay (see red dashed line). Using these two controls help us to identify a variation of the background signal upon addition of the miRNA extracted from human serum, and to roughly quantify this variation, which can led us to identify its origin. Thus, when comparing both background signals, it is possible to notice how it increases upon addition of the miRNA pool from human serum. Interestingly, when quantifying this increment in the background signal, we found out that it was close to the signal produced by a concentration of target sequence of around 50 fM. It is noteworthy that similar concentration values for miR-21-5p extracted from healthy patients (around 30 fM) have been previously reported by other authors [49]. This result could indicate that our sensor is detecting the miR-21-5p concentration that is naturally present on a serum sample extracted from a healthy patient. Although this result should be taken with caution, it is encouraging given the potential possibilities offered by affordable detection platforms like the one presented here, which can be built where and when needed by 3D-printing technologies. Additionally, it is important to highlight that the lowest concentration that is able to be distinguished in these conditions (i.e. around 50 fM), is in any case below the miR-21-5p concentrations present in the serum of breast cancer patients as reported elsewhere [50,49]. This implies that the increased miR-21-5p serum concentration present in these patients (89–102 fM) may be easily distinguished with the proposed sensor. As a final remark, when compared with similar detection platforms reported in literature based on UCNP and magnetic beads, this strategy permits a sensitivity 5-fold greater than those reported in literature [30–34]. More specifically, to the best of our knowledge it represents a more than 400-fold improvement when compared with reports that aim to detect DNA sequences as the target analyte [33–36]. The ultrasensitivity of the proposed sensor can be explained by the reduction in the non-specific binding of the UC Probe reporter to the solid support, as this is directly responsible for the background signal intensity, due to the lack of autofluorescence provided in biological media by the UCNP's anti-Stokes emissions. The reduction of non-specific binding is achieved in our strategy thanks to the composition of the assay buffer (i.e. high concentration of bovine serum

albumin (BSA) and surfactant), combined with the use of a photoligation strategy that allows repeated and more stringent washes. In order to give a more comprehensive picture of why non-specific binding of the reporter is a major factor limiting ultrasensitivity in this kind of sensors, a theoretical estimation of its impact on the assay experimental response is presented next.

3.2. Estimation of sensor response based on equilibrium ligand binding assays: The importance of non-specific binding on sensor's sensitivity

We theoretically reproduced the experimental response of our oligonucleotide sensor by using the Hill or Langmuir equation that quantifies the ligand-receptor (target-UC Probe) interactions for ligand binding assays [38,39,51]. This is derived from the law of mass action:

$$nT + UC \xrightleftharpoons[k_2]{k_1} T_nUC, \tag{1}$$

where n binding sites of the receptor UC (UC Probe) are available for the ligand T (target). For the sake of simplicity, we did not consider partial receptor occupancy, only the final complex T_nUC which accounts for the UC Probes which finally were collected by the magnetic particles and therefore contributed to the luminescence signal. The parameters k_1 and k_2 are the association and dissociation rate constants. At the equilibrium, the molar concentration of the complex target-UC Probe $[T_nUC]$ follows the well-known Hill-Langmuir equation [38,39]:

$$[T_nUC] = [UC_0] \frac{[T]^n}{[T]^n + (K_E)^n}, \tag{2}$$

where $[UC_0]$ is the total molar concentration of UC Probes and $[T]$ is the total molar concentration of target. $(K_E)^n = k_2/k_1$, where K_E is the target concentration at which half of the UC Probes are bound to targets. For the case of one binding site $n = 1$, this parameter equals the equilibrium dissociation constant of the target-UC Probe complex $K_d = k_2/k_1$. For target concentrations below K_E , the target-UC Probe complex concentration $[T_nUC]$ follows a power law with $[T]$ with an exponent equal to n . This n value is the well-known Hill coefficient which presents a more general interpretation than the original one as the number of binding sites [38]. Therefore, $[T_nUC]$ versus $[T]$ exhibits a linear trend in a log-log plot which leads the sensor calibration response. At higher concentrations of target, $[T]$ above K_E , the concentration of target-UC Probe complex $[T_nUC]$ saturates reaching a plateau where all the UC Probes are bound to targets and therefore, it deviates from the above mentioned linear behavior. As an example, we plot in Fig. 7 (dashed line) the fraction of UC Probes captured by the target $[T_nUC]/[UC_0]$ as a function of the

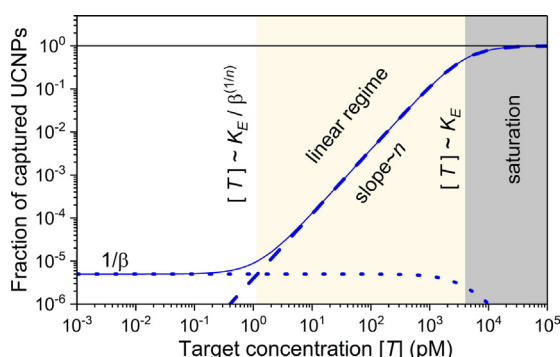


Fig. 7. Theoretical fraction of captured UC Probes versus the total target concentration $[T]$ in a log-log plot. Dashed line represents the concentration of target-UC Probe complex $[T_nUC]$ normalized to the concentration of UC Probes $[UC_0]$ and exhibits the typical linear regime up to a saturation for $[T]$ above K_E .

target concentration $[T]$ in a log-log plot. Our model is able to reproduce the experimental findings with a very good agreement by considering a Hill coefficient $n = 1.5$ (matching the fitting slope of the experimental data) and a value of $K_E = 4000$ pM to ensure the linear regime to be present until the tens of nanomolar range of target.

Now we must take into account that the luminescence signal measured in the control sample (without target) comes from UC Probes non-specifically adsorbed onto the surface of Mag Probes, that is, non-specific binding. This can be accounted by the following equilibrium chemical reaction:

$$UC \xrightleftharpoons[\beta_2]{\beta_1} UC^*, \tag{3}$$

which gives us the concentration of UC Probes physisorbed to the Mag Probes $[UC^*]$:

$$[UC^*] = \frac{1}{1 + \beta} ([UC_0] - [T_nUC]), \tag{4}$$

where $\beta = \beta_2/\beta_1$, being β_1 and β_2 the non-specific association and dissociation rate constants. For the case without target, the fraction of non-specific captured UC Probes $[UC^*]/[UC_0] \approx 1/\beta$ will be responsible of the control luminescence signal. That means the parameter β gives us the experimental control signal value. Dotted line in Fig. 7 shows the fraction of non-specific captured UC Probes $[UC^*]/[UC_0]$ (Eq. 4) for a value of $\beta = 2 \times 10^5$. The curve shows a nearly constant value close to $\approx 1/\beta$, i.e. the one achieved without target. At high target concentrations, in the saturation regime $[T] > K_E$, the number of non-specifically bound UC Probes decreases since most of the UC Probes are easily target-binding. Finally, the total concentration of captured UC Probes is shown in Fig. 7 (solid line) which is the sum of both contributions: $[T_nUC] + [UC^*]$. The offset value given by Eq. 4 roughly imposes the lower limit of the target concentration range exhibiting the linear trend of the sensor. It happens where the number of target-UC Probe complexes becomes similar to the number of non-specific UC Probes captured by the Mag Probes. This occurs at a target concentration value close to $[T] \approx K_E/\beta^{1/n}$ below which the signal approaches to the control value. Using the parameter values of Fig. 7 we obtain that the value of $[T]$ is ≈ 1 pM. This estimation reflects that the major restriction to detect smaller target concentrations is the non-specific binding. Following this reasoning we were able to roughly reproduce the behavior of the experimental data as shown in Figs. 4 and 6. There, the fraction of captured UC Probes $[T_nUC]/[UC_0] + [UC^*]/[UC_0]$ (see Eqs. 2 and 4) is shown by using the above mentioned parameters $n = 1.5$ and $K_E = 4000$ pM. We chose the value of β to properly reproduce the corresponding control value for each experiment. In Fig. 4 we used $\beta = 2.5 \times 10^5$ which leads to a lower limit value as the one mentioned above, $[T] \approx 1$ pM. As shown in Fig. 6, the photoligation process seems to reduce indeed the control signal, in agreement with our theoretical estimation of $\beta = 8 \times 10^5$ which leads to a lower limit of $[T] \approx 0.5$ pM. Therefore, the reduction of non-specific binding allows to detect smaller target concentrations, and stands out as one of the key drawbacks to overcome in order to keep developing direct detection assays with increasingly higher ultrasensitivities. In this regard, photoligation seems to be a very suitable strategy to overcome this limitation in oligonucleotide detection platforms, as the covalent linkage formed between the UC Probe and the Mag Probe allows to conserve this target-specific signal upon thorough washes, even when the DNA duplex between the target and the probes is denatured, while the non-specifically bound luminescent reporters (UC Probes) are removed upon washes. This results in an improvement of the S/B ratio and the assay LOD. More interestingly, photoligation is susceptible to be combined with additional strategies that aim to reduce non-specific binding by using other mechanisms. In this regard we

may classify photoligation as a post-“non-specific binding” strategy, as it allows to reduce this effect once it has taken place. By contrast, most previous strategies have traditionally focused on preventing non-specific binding to occur, which may be classified as a pre-“non-specific binding” strategy. This can be achieved by introducing molecules in the assay buffer that mimic the surface chemical properties of the reporter and compete with them towards possible non-specific binding sites [52], or modifying the surface of the solid support and/or the reporter with anti-fouling molecules (e.g. PEGs) that reduce the strength of these non-specific interactions [53,54]. Thus, we advance that designing detection assays that simultaneously combine both pre- and post-“non-specific binding” treatments may prove synergistic regarding the development of assays featuring a further improved ultrasensitivity, as well as a better dynamic range, reproducibility and selectivity [54].

4. Conclusions

In this work, we developed and optimized a luminescence sensing platform for the detection of specific oligonucleotide sequences. The mechanism of the sensor is based on the capture of photoluminescent ssDNA-UCNPs by ssDNA-magnetic microparticles upon hybridization with the targeted DNA complementary sequence. At this point, a photoligation step links covalently the ssDNA from the UCNPs to the ssDNA from the magnetic microparticles, which were held face to face upon hybridization with the target sequence. This covalent bond allowed the use of more stringent washes during the assay, which translated in an 10-fold improvement of its limit of detection (i.e. from 500 fM to less than 50 fM). To the best of our knowledge this represents a more than 400-fold improvement when compared with similar platforms to detect DNA sequences reported in literature [33–36]. We found that a proper compromise between the number of magnetic microparticles used during the assay, and the area in which the UCNPs-magnetic microparticles complexes were concentrated to read the result, was important to achieve a good detectability of the UCNPs reporters luminescence. The use of larger UCNPs proved to be also beneficial, as the power density required to read the assays could be reduced 3-fold. This can be suitable for both, the use of a less powerful and more portable excitation source, and to avoid potential sample degradation effects. The optimized sensor was finally tested in samples that contained total miRNA extracted from human serum. Under these conditions, the sensor maintained most of the analytical characteristics featured in the absence of extracted total miRNA, such as its LOD (less than 50 fM), linear range (more than two orders of magnitude), and slope of 1.6. This result is encouraging, since indicates the suitability of the presented platform to detect the presence of miR-21-5p at concentrations present in the serum of breast cancer patients [50,49] and even more the concentration naturally present on healthy patients [49]. The possibility to quickly modify and print most of the setup required for the detection assay at an affordable price, at any time, and any location worldwide (given that there is a 3D-printing spot nearby), is an additional advantage of 3D-printed sensing platforms. Finally, we theoretically demonstrated, by following the proposed model for ligand binding assays, that a major factor limiting the sensor sensitivity is non-specific binding. In this direction, photoligation strategies, and probably its combination with other additional approaches that may help to reduce this effect at maximum, seem to be very suitable to achieve ultrasensitive sensors when taking advantage of the autofluorescence-free luminescence from UCNPs.

CRediT authorship contribution statement

Diego Mendez-Gonzalez: Conceptualization, Investigation, Writing - original draft, Writing - review & editing. **Pedro P. Silva-Ibáñez:** Investigation. **Fernando Valiente-Dies:** Investiga-

tion. **Oscar G. Calderón:** Investigation, Software, Writing - original draft, Writing - review & editing. **Juan L. Mendez-Gonzalez:** Investigation. **Marco Laurenti:** Writing - review & editing. **Ana Egatz-Gómez:** Writing - review & editing. **Elena Díaz:** Writing - review & editing, Funding acquisition. **Jorge Rubio-Retama:** Conceptualization, Writing - review & editing, Supervision, Funding acquisition. **Sonia Melle:** Investigation, Writing - original draft, Writing - review & editing, Funding acquisition.

Declaration of Competing Interest

The authors declare that they have no known competing financial interests or personal relationships that could have appeared to influence the work reported in this paper.

Acknowledgments

This work was supported by Ministerio de Economía y Competitividad (MAT2017-83111R and PID2019-106820RB-C21), Ministerio de Ciencia, Innovación, y Universidades (MICINN, RTI2018-094859) and Comunidad de Madrid (B2017/BMD-3867 RENIM-CM) co-financed by European Structural and Investment Fund. D.M.G. thanks UCM-Santander for a predoctoral contract (CT17/17-CT18/17) and a Postdoctoral Orientation Period (POP) contract. P. S. I. thanks CONICYT for a predoctoral contract (N° 21161052). F. V. D. thanks to European Commission for a YEI program contract (PEJD-2018-PRE/IND-9118). TEM images were obtained at the National Center for Electron Microscopy (UCM, Madrid) facility.

Appendix A. Supplementary material

Supplementary data associated with this article can be found, in the online version, at <https://doi.org/10.1016/j.jcis.2021.02.093>.

References

- [1] J. Hayes, P.P. Peruzzi, S. Lawler, MicroRNAs in cancer: biomarkers, functions and therapy, *Trends Mol. Med.* 20 (8) (2014) 460–469.
- [2] S. Maciotta Rolandin, M. Meregalli, Y. Torrente, The involvement of microRNAs in neurodegenerative diseases, *Front. Cell. Neurosci.* 7 (2013) 265.
- [3] A. Grundhoff, C.S. Sullivan, Virus-encoded microRNAs, *Virology* 411 (2) (2011) 325–343.
- [4] E. Girardi, P. López, S. Pfeffer, On the Importance of Host MicroRNAs During Viral Infection, *Front. Genet.* 9 (2018) 439. ISSN 0003-2670.
- [5] W.P. Kloosterman, R.H. Plasterk, The Diverse Functions of microRNAs in Animal Development and Disease, *Develop. Cell* 11 (4) (2006) 441–450, ISSN 1534-5807.
- [6] Y. Han, H. Li, miRNAs as biomarkers and for the early detection of non-small cell lung cancer (NSCLC), *J. Thoracic Disease* 10 (5) (2018) 3119–3131.
- [7] C. Sanfiorenzo, M.I. Ilie, A. Belaid, F. Barlési, J. Mouroux, C.-H. Marquette, P. Brest, P. Hofman, Two panels of plasma microRNAs as non-invasive biomarkers for prediction of recurrence in resectable NSCLC, *PLOS ONE* 8 (1) (2013) 1–8.
- [8] C.E. Condrat, D.C. Thompson, M.G. Barbu, O.L. Bugnar, A. Boboc, D. Cretoiu, N. Suci, S.M. Cretoiu, S.C. Voinea, miRNAs as biomarkers in disease: latest findings regarding their role in diagnosis and prognosis, *Cells* 9 (2) (2020) 276, ISSN 2073-4409.
- [9] G.-K. Wang, J.-Q. Zhu, J.-T. Zhang, Q. Li, Y. Li, J. He, Y.-W. Qin, Q. Jing, Circulating microRNA: a novel potential biomarker for early diagnosis of acute myocardial infarction in humans, *Eur. Heart J.* 31 (6) (2010) 659–666.
- [10] M.R. Hartman, R.C.H. Ruiz, S. Hamada, C. Xu, K.G. Yancey, Y. Yu, W. Han, D. Luo, Point-of-care nucleic acid detection using nanotechnology, *Nanoscale* 5 (2013) 10141–10154.
- [11] P. Guan, Z. Yin, X. Li, W. Wu, B. Zhou, Meta-analysis of human lung cancer microRNA expression profiling studies comparing cancer tissues with normal tissues, *J. Exp. Clin. Cancer Res.* 31 (54) (2012) 1–8.
- [12] A. Egatz-Gomez, C. Wang, F. Klacsmann, Z. Pan, S. Marczak, Y. Wang, G. Sun, S. Senapati, H.-C. Chang, Future microfluidic and nanofluidic modular platforms for nucleic acid liquid biopsy in precision medicine, *Biomicrofluidics* 10 (3) (2016) 032902.
- [13] Z. Farka, M.J. Mickert, A. Hlaváček, P. Skládal, H.H. Gorris, Single molecule upconversion-linked immunosorbent assay with extended dynamic range for the sensitive detection of diagnostic biomarkers, *Anal. Chem.* 89 (21) (2017) 11825–11830.
- [14] V. Kale, H. Pääkkilä, J. Vainio, A. Ahomaa, N. Sirkka, A. Lyytikäinen, S.M. Talha, A. Kutsaya, M. Waris, I. Julkunen, T. Soukka, Spectrally and spatially multiplexed

- serological array-in-well assay utilizing two-color upconversion luminescence imaging, *Anal. Chem.* 88 (8) (2016) 4470–4477.
- [15] D. Mendez-Gonzalez, S. Lahtinen, M. Laurenti, E. López-Cabarcos, J. Rubio-Retama, T. Soukka, Photochemical ligation to ultrasensitive DNA detection with upconverting nanoparticles, *Anal. Chem.* 90 (22) (2018) 13385–13392.
- [16] V. Poláčková, M. Pastucha, Z. Mikušová, M.J. Mickert, A. Hlaváček, H.H. Gorris, P. Skládal, Z. Farka, Click-conjugated photon-upconversion nanoparticles in an immunoassay for honeybee pathogen *Melissococcus plutonius*, *Nanoscale* 11 (2019) 8343–8351.
- [17] A. Nadort, J. Zhao, E.M. Goldys, Lanthanide upconversion luminescence at the nanoscale: fundamentals and optical properties, *Nanoscale* 8 (2016) 13099–13130.
- [18] C. Duan, L. Liang, L. Li, R. Zhang, Z.P. Xu, Recent progress in upconversion luminescence nanomaterials for biomedical applications, *J. Mater. Chem. B* 6 (2018) 192–209.
- [19] S. Wen, J. Zhou, K. Zheng, A. Bednarkiewicz, X. Liu, D. Jin, Advances in highly doped upconversion nanoparticles, *Nature Commun.* 9 (2415) (2018) 1–12.
- [20] D. Mendez-Gonzalez, S. Melle, O.G. Calderón, M. Laurenti, E. Cabrera-Granado, A. Egatz-Gómez, E. López-Cabarcos, J. Rubio-Retama, E. Díaz, Control of upconversion luminescence by gold nanoparticle size: from quenching to enhancement, *Nanoscale* 11 (2019) 13832–13844.
- [21] D. Mendez-Gonzalez, O.G. Calderón, S. Melle, J. González-Izquierdo, L. Bañares, D. López-Díaz, M.M. Velázquez, E. López-Cabarcos, J. Rubio-Retama, M. Laurenti, Contribution of resonance energy transfer to the luminescence quenching of upconversion nanoparticles with graphene oxide, *J. Colloid Interface Sci.* 575 (2020) 119–129. ISSN 0021-9797.
- [22] Q. Ju, U. Udayasankar, U. Krull, Paper-based DNA detection using lanthanide-doped LiYF₄ upconversion nanocrystals as bioprobe, *Small* 10 (19) (2014) 3912–3917.
- [23] M.-K. Tsang, W. Ye, G. Wang, J. Li, M. Yang, J. Hao, Ultrasensitive detection of Ebola virus oligonucleotide based on upconversion nanoprobe/nanoporous membrane system, *ACS Nano* 10 (1) (2016) 598–605.
- [24] D. Mendez-Gonzalez, E. Lopez-Cabarcos, J. Rubio-Retama, M. Laurenti, Sensors and bioassays powered by upconverting materials, *Adv. Colloid Interface Sci.* 249 (2017) 66–87.
- [25] Z. Saberi, B. Rezaei, T. Khayamian, A fluorescent aptasensor for analysis of adenosine triphosphate based on aptamer-magnetic nanoparticles and its single-stranded complementary DNA labeled carbon dots, *Luminescence* 33 (4) (2018) 640–646.
- [26] M. Bao, E. Jensen, Y. Chang, G. Korensky, K. Du, Magnetic Bead-Quantum Dot (MB-Qdot) clustered regularly interspaced short palindromic repeat assay for simple viral DNA detection, *ACS Appl. Mater. Interfaces* 12 (39) (2020) 43435–43443.
- [27] V. Mani, B.V. Chikkaveeriah, J.F. Rusling, Magnetic particles in ultrasensitive biomarker protein measurements for cancer detection and monitoring, *J. Expert Opin. Med. Diagnost.* 5 (2011) 381–391.
- [28] S. Fang, C. Wang, J. Xiang, L. Cheng, X. Song, L. Xu, R. Peng, Z. Liu, Aptamer-conjugated upconversion nanoprobe assisted by magnetic separation for effective isolation and sensitive detection of circulating tumor cells, *Nano Res.* 7 (9) (2014) 1327–1336.
- [29] L.-F. Jiang, B.-C. Chen, B. Chen, X.-J. Li, H.-L. Liao, H.-M. Huang, Z.-J. Guo, W.-Y. Zhang, L. Wu, Detection of Aβ oligomers based on magnetic-field-assisted separation of aptamer-functionalized Fe₃O₄ magnetic nanoparticles and BaYF₅:Yb, Er nanoparticles as upconversion fluorescence labels, *Talanta* 170 (2017) 350–357.
- [30] S. Wu, N. Duan, Z. Wang, H. Wang, Aptamer-functionalized magnetic nanoparticle-based bioassay for the detection of ochratoxin A using upconversion nanoparticles as labels, *Analyst* 136 (2011) 2306–2314.
- [31] N. Sun, Y. Ding, Z. Tao, H. You, X. Hua, M. Wang, Development of an upconversion fluorescence DNA probe for the detection of acetamiprid by magnetic nanoparticles separation, *Food Chem.* 257 (2018) 289–294. ISSN 0308-8146.
- [32] Y. Li, Z. Wu, Z. Liu, An immune sandwich assay of carcinoembryonic antigen based on the joint use of upconversion phosphors and magnetic beads, *Analyst* 140 (2015) 4083–4088.
- [33] L.V. Wollenberger, Y.-M.M. Yao, N.A. Mufti, L.V. Schneider, Detection of DNA using upconverting phosphor reporter probes, in: G.E. Cohn, G.E. Cohn, S.A. Soper (Eds.), *Ultrasensitive Biochemical Diagnostics II*, vol. 2985, SPIE International Society for Optics and Photonics, 1997, pp. 100–111.
- [34] L. Wang, Y. Li, Green upconversion nanocrystals for DNA detection, *Chem. Commun.* (2006) 2557–2559.
- [35] S. Wu, N. Duan, X. Ma, Y. Xia, Y. Yu, Z. Wang, H. Wang, Simultaneous detection of enterovirus 71 and coxsackievirus A16 using dual-colour upconversion luminescent nanoparticles as labels, *Chem. Commun.* 48 (2012) 4866–4868.
- [36] S. Wu, N. Duan, X. Ma, Y. Xia, Y. Yu, Z. Wang, H. Wang, Simultaneous detection of enterovirus 71 and coxsackievirus A16 using dual-colour upconversion luminescent nanoparticles as labels, *Chem. Commun.* 48 (2012) 4866–4868.
- [37] P.R. Potluri, V.K. Rajendran, C.T. Tran, D.R. McKenzie, A. Sunna, Linker-protein G mediated functionalization of polystyrene-encapsulated upconversion nanoparticles for rapid gene assay using convective PCR, *Microchim. Acta* 186 (2019) 346.
- [38] R. Gesztelyi, J. Zsuga, A. Kemeny-Beke, B. Varga, B. Juhasz, A. Tosaki, The Hill equation and the origin of quantitative pharmacology, *Arch. Hist. Exact Sci.* 66 (4) (2012) 427–438.
- [39] J. Giraldo, N.M. Vivas, E. Vila, A. Badia, Assessing the (a)symmetry of concentration-effect curves: empirical versus mechanistic models, *Pharmacol. Therapeut.* 95 (1) (2002) 21–45.
- [40] Z. Li, Y. Zhang, An efficient and user-friendly method for the synthesis of hexagonal-phase NaYF₄:Yb, Er/Tm nanocrystals with controllable shape and upconversion fluorescence, *Nanotechnology* 19 (34) (2008) 345606.
- [41] L.E. Mackenzie, J.A. Goode, A. Vakurov, P.P. Nampi, S. Saha, G. Jose, P.A. Millner, The theoretical molecular weight of NaYF₄:RE upconversion nanoparticles, *Sci. Rep.* 8 (1) (2018) 1106.
- [42] S. Nakamura, S. Ogasawara, S. Matuda, I. Saito, K. Fujimoto, Template directed reversible photochemical ligation of oligodeoxynucleotides, *Molecules* 17 (1) (2011) 163–178.
- [43] K. Fujimoto, N. Ogawa, M. Hayashi, S. Matsuda, I. Saito, Template directed photochemical synthesis of branched oligodeoxynucleotides via 5-carboxyvinyl deoxyuridine †Dedicated to Professor Harry H. Wasserman on the occasion of his 80th birthday†, *Tetrahedron Lett.* 41 (49) (2000) 9437–9440.
- [44] K. Fujimoto, S. Matsuda, N. Takahashi, I. Saito, Template-Directed Photoreversible Ligation of Deoxyoligonucleotides via 5-Vinyldeoxyuridine, *J. Am. Chem. Soc.* 122 (23) (2000) 5646–5647.
- [45] R.L. McCally, Measurement of Gaussian Beam Parameters, *Appl. Opt.* 23 (14) (1984) 2227.
- [46] P. Hänninen, H. Härmä (Eds.), *Lanthanide Luminescence Photophysical, Analytical and Biological Aspects*. In Springer Series on Fluorescence, vol. 7, Springer Verlag, 2011.
- [47] T. Näreoja, M. Vehniäinen, U. Lamminmäki, P.E. Hänninen, H. Härmä, Study on nonspecificity of an immunoassay using Eu-doped polystyrene nanoparticle labels, *J. Immunol. Methods* 345 (1) (2009) 80–89.
- [48] J.-C. Boyer, F.C.J.M. van Veggel, Absolute quantum yield measurements of colloidal NaYF₄: Er³⁺, Yb³⁺ upconverting nanoparticles, *Nanoscale* 2 (2010) 1417–1419.
- [49] M. Zouari, S. Campuzano, J.M. Pingarrón, N. Raouafi, Femtomolar direct voltammetric determination of circulating miRNAs in sera of cancer patients using an enzymeless biosensor, *Anal. Chim. Acta* 1104 (2020) 188–198.
- [50] M. Zouari, S. Campuzano, J.M. Pingarrón, N. Raouafi, Amperometric biosensing of miRNA-21 in serum and cancer cells at nanostructured platforms using Anti-DNA–RNA hybrid antibodies, *ACS Omega* 3 (8) (2018) 8923–8931.
- [51] E.C. Hulme, M.A. Trevethick, Ligand binding assays at equilibrium: validation and interpretation, *Br. J. Pharmacol.* 161 (6) (2010) 1219–1237.
- [52] S. Lahtinen, A. Lyytikäinen, N. Sirkka, H. Pääkkilä, T. Soukka, Improving the sensitivity of immunoassays by reducing non-specific binding of poly(acrylic acid) coated upconverting nanoparticles by adding free poly(acrylic acid), *Microchim. Acta* 185 (4) (2018) 1436–5073.
- [53] T. Pochechueva, A. Chinarev, N. Bovin, A. Fedier, F. Jacob, V. Heinzelmann-Schwarz, PEGylation of microbead surfaces reduces unspecific antibody binding in glycan-based suspension array, *J. Immunol. Methods* 412 (2014) 42–52.
- [54] J.Y. Lichtenberg, Y. Ling, S. Kim, Non-specific adsorption reduction methods in biosensing, *Sensors* 19 (2019) 2488.